LIMNOLOGY and OCEANOGRAPHY

ASLO

Limnol. Oceanogr. 62, 2017, 1620–1635

doi: 10.1002/lno.10521

Winter weather and lake-watershed physical configuration drive phosphorus, iron, and manganese dynamics in water and sediment of ice-covered lakes

DongJoo Joung,[1]* Meagan Leduc,[2,7] Benjamin Ramcharitar,[3] Yaoyang Xu,[1] Peter D. F. Isles,[1,4] Jason D. Stockwell,[4] Gregory K. Druschel,[5] Tom Manley,[6] Andrew W. Schroth[1,7]

[1]EPSCoR, University of Vermont, Burlington, Vermont
[2]Department of Natural Science, Lyndon State College, Lyndonville, Vermont
[3]Department of Biology, Middlebury College, Middlebury, Vermont
[4]Rubenstein Ecosystem Science Laboratory, University of Vermont, Burlington, Vermont
[5]Department of Earth Science, Indiana University Purdue University Indianapolis (IUPUI), Indianapolis, Indiana
[6]Department of, Geology, Middlebury College, Middlebury, Vermont
[7]Department of Geology, University of Vermont, Burlington, Vermont

Abstract

While decreasing occurrence and duration of lake ice cover is well-documented, biogeochemical dynamics in frozen lakes remain poorly understood. Here, we interpret winter physical and biogeochemical time series from eutrophic Missisquoi Bay (MB) and hyper-eutrophic Shelburne Pond (SP) to describe variable drivers of under ice biogeochemistry in systems of fundamentally different lake-watershed physical configurations (lake area, lake : watershed area). The continuous cold of the 2015 winter drove the MB sediment-water interface to the most severe and persistent suboxic state ever documented at this site, promoting the depletion of redox-sensitive phases in sediments, and an expanding zone of bottom water enriched in reactive species of Mn, Fe, and P. In this context, lake sediment and water column inventories of reactive chemical species were sensitive to the severity and persistence of subfreezing temperatures. During thaws, event provenance and severity impact lake thermal structure and mixing, water column enrichment in P and Fe, and thaw capability to suppress redox front position and internal chemical loading. Nearly identical winter weather manifest differently in nearby SP, where the small surface and watershed areas promoted a warmer, less stratified water column and active phytoplankton populations, impacting biogeochemical dynamics. In SP, Fe and P behavior under ice were decoupled due to active biological cycling, and thaw impacts were different in distribution and composition due to SP's physical structure and related antecedent conditions. We find that under ice biogeochemistry is highly dynamic in both time and space and sensitive to a variety of drivers impacted by climate change.

Global climate change has and will continue to cause a reduction in the frequency and duration of ice cover during winter (IPCC 2007; Weyhenmeyer et al. 2008, 2011; Dibike et al. 2012; Shuter et al. 2013). Many seasonally ice covered lakes ranging from small ponds to the Laurentian Great Lakes have experienced delayed ice-onset and early ice break-up (Magnuson et al. 2000; Hodgkins et al. 2002; Vincent 2010). Variation in duration and timing of ice cover can be important for physical and biogeochemical processes such as water column mixing, internal nutrient loading, and biological production and community composition (Adrian et al. 1999, 2009; Weyhenmeyer et al. 1999; Jackson et al. 2007; Bruesewitz et al. 2015). However, studies that integrate physical, biogeochemical and ecological under ice dynamics across both temporal and spatial gradients are absent in the literature, but likely critical to understand how lake water quality and ecological function will respond to the global climate change.

Biogeochemical conditions under ice may be heavily influenced by hydrodynamic conditions, and these conditions are likely to change over the course of the winter as a

*Correspondence: djoung@uvm.edu or dongjoojoung@gmail.com

Additional Supporting Information may be found in the online version of this article.

result of changing temperature and hydrologic inputs. During periods of persistent sub-freezing air temperatures, lake hydrodynamic conditions are generally characterized by minimal water movement because of the suppression of wind-forcing and minimal river water influx (Bengtsson 1996). Limited hydrodynamic mixing under ice promotes stratified water column temperature profiles, with temperatures near zero directly underneath the ice and warmer temperatures toward the sediment water interface (SWI) (Fang and Stefan 1996). Typically, dissolved oxygen (DO) is gradually depleted toward the lake bottom due to decomposition of organic matter near the SWI (Babin and Prepas 1985) coupled with limited mixing and ice cover suppressed oxygen input from atmosphere (Bruesewitz et al. 2015). Under these conditions, benthic heterotrophic respiration can promote progressively reducing conditions across the SWI (Karlsson et al. 2008; Gammons et al. 2014; Manasypov et al. 2014; Schroth et al. 2015).

As reducing conditions in sediments and water become stronger, redox-sensitive metals (Fe, Mn) and associated nutrients (P) can be re-mobilized from their particulate forms (Davison 1993; Martin 2005). When Fe and Mn nanoparticles are reductively dissolved, sorbed P can be released (Shiller 2003; Søndergaard et al. 2003), resulting in enrichment of bottom water Fe, Mn, and P in lakes with an-/suboxic conditions (Balistrieri et al. 1992; Søndergaard et al. 2003; Brown et al. 2013; Nürnberg et al. 2013). Conversely, in oxygenated water and sediments Mn(II) and Fe(II) can be rapidly oxidized, forming high surface concentrations of Mn(IV) and Fe(III) (hydr)oxides, which can rapidly scavenge available orthophosphate (Kawashima et al. 1986; Martin 2005; Zaman et al. 2013). Particle sizes of the Fe and Mn (hydr)oxides will also evolve in time and coarsen through nanoparticulate and colloidal fractions, and these processes may be impacted by a variety of factors such as temperature, pH, and the concentrations of ligands (Davison and Seed 1983; Gunnars et al. 2002; Gilbert et al. 2003; Martin 2005). During extended subfreezing periods, the evolution of metal and nutrient pools under ice cover are likely to be controlled by the progressive development of reducing conditions in bottom waters.

Thaw events can have significant impacts on both geochemical and hydrodynamic conditions in receiving waters, in that the runoff water and solutes can have very different biogeochemical properties associated with watershed processes and provenance (Schroth et al. 2015). Additionally, thaws have been demonstrated to be particularly enriched in watershed-derived solutes such as dissolved organic carbon (DOC), N, P, and Fe, suggesting that thaws may be particularly important in providing reactive phases of many constituents to the under ice system (Schroth et al. 2015). Furthermore, the concentration and distribution of chemical constituents will be impacted by typical drivers of watershed biogeochemistry such as land cover, antecedent conditions, and thaw event severity and duration (Winston et al. 1995; Brooks and Williams 1999; Meixner and Bales 2003). Progressive snow melting also delivers different chemical constituents, in that some chemical constituents (e.g., N, S) in watersheds can elute faster than others (e.g., Cl) due to evolving provenance of the thaw meltwater (Catalan 1992). Schroth et al. (2015) observed an increased influx of Fe and P under ice during thaw periods, with concentrations at least 4–5 times higher than the concentrations during the preceding conditions. Thus, understanding the nature of watershed inputs during thaw periods could be very important to project impacts of winter dynamics on spring and summer biogeochemistry and ecology in lakes.

Biological activities can also impact under ice dynamics of nutrient and metals due to uptake and remineralization as well as through manipulation of pH and oxygen dynamics (production and respiration) (Bertilsson et al. 2013). Because considerable phytoplankton productivity has been observed under ice, impacts of these populations on geochemical dynamics are likely in productive under ice systems (Vincent 1981; Bertilsson et al. 2013; Manasypov et al. 2014). Furthermore, light availability is known to be a predominant control for under ice biological production (Leppäranta 2014), and thus ice thickness and snow cover can potentially be critical drivers of under ice biogeochemical dynamics through mediating biological productivity and distribution.

Overall, under-ice biogeochemical cycles of metals and nutrients are complicated processes influenced by SWI redox status, water column ecology, hydrodynamics, and watershed processes, which are all highly variable in time and space in lakes. Furthermore, all of these drivers are likely impacted by the severity and duration of winter weather. However, integrated studies of physical, biogeochemical, and ecological under-ice dynamics are noticeably absent from the literature, but critical for understanding the consequences of the global climate change on lake systems. Here, we interpret hydrodynamic, biogeochemical, and ecological monitoring data from a well-studied eutrophic site, Missisquoi Bay (MB) of Lake Champlain, during the 2015 winter and compare these data to a similar and concurrent data set collected from hyper-eutrophic Shelburne Pond (SP), Vermont. Our overarching goal in this comparison was to examine how two shallow lake systems with very different lake-watershed physical configurations (lake surface area, watershed : lake area ratio) impact P, Fe, and Mn dynamics in under-ice water and sediment columns when exposed to the same winter weather. A secondary objective of this work is to compare biogeochemical dynamics under the ice of MB in the less persistently severe (slower ice growth, more mid-winter above freezing episodes and thaw events) winter of 2014 (Schroth et al. 2015) to those of the winter of 2015, characterized by historically persistent subfreezing temperatures. This comparison allows us to examine the impact of inter-annual variability in winter weather on under ice biogeochemical dynamics at the same monitoring site using the same methods.

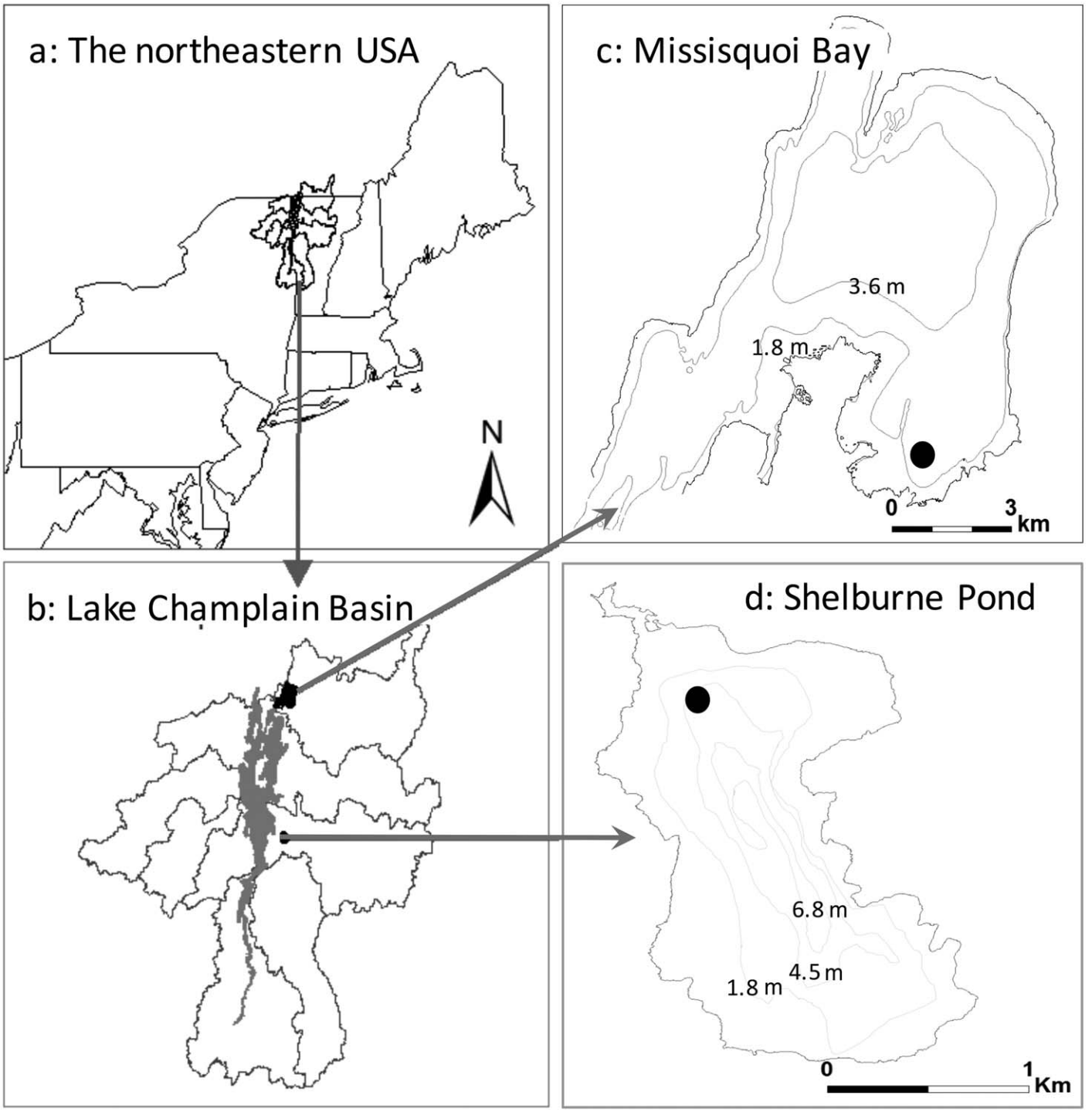

Fig. 1. Map of **a**) the northeastern USA, **b**) Lake Champlain Basin, **c**) Missisquoi Bay and **d**) Shelburne Pond. Shelburne Pond is located about 80 km south of the Missisquoi Bay.

Methods and materials

Site description

Shelburne Pond (SP) and Missisquoi Bay (MB) are hypereutrophic and eutrophic systems, respectively, with persistent cyanobacterial blooms that occur primarily in the summer due to historical and current anthropogenic nutrient loading from their catchments (Ferber et al. 2004; Lini et al. 2007; Levine et al. 2012). Shelburne Pond is located 80 km south of MB (Fig. 1) at similar elevation (Table 1) and exposed to similar weather patterns and events. The physical

Table 1. Missisquoi Bay and Shelburne Pond lake-watershed physical properties.

	Waterbody			Watershed	
	MB	SP		MB	SP
Surface area (km^2)	77.5	1.8	Total area (km^2)	3105	19
Mean depth (m)	2.8	3.4	Forest (%)	62	78
Max depth (m)	4	7.6	Agriculture (%)	25	15
Volume (km^3)	0.22	0.007	Urban (%)	5	7

*Reference (Ferber et al. 2004; Levine et al. 2012; Vermont Department of Environmental Conservation (VTDEC) 2014).

dimensions of MB are much larger than SP, though maximum and mean depths are lower than SP (Table 1). The watershed of MB (3100 km^2) is primarily forested (70% of the catchment), followed by agricultural (25%) and urban (5%) areas, with three river systems (Missisquoi, Pike, and Rock) entering the bay. The small watershed of SP (19 km^2) does not have a major tributary and is covered by 78% forest and 15% agriculture.

Water and sediment analysis

Under-ice water and sediment samples were collected at the same site in MB and SP during eight sampling trips from 15th January (Julian date: JD 15) to 6th April (JD 97) in 2015. We note that water and sediment sample collections as well as sensor measurements in 2015 winter followed the same techniques applied in 2014 winter sampling in MB, which is detailed in Schroth et al. (2015). Multiple holes through the ice were drilled to measure ice thickness, make water column profile measurements with a sonde (duplicate castes in different holes), and collect water samples and two sediment cores. Holes were 1–2 m away from each other to minimize contamination and disturbance among sample collections and sensor measurements.

Duplicate water column sensor measurements using a YSI 6600 sonde (YSI, Yellow Springs, Ohio) for temperature, DO, pH, conductivity, chlorophyll *a*, and phycocyanin were recorded every 0.5 m from just under the ice to the SWI through two holes. The sensor was calibrated prior to sampling using manufacturer's instructions. The near-bottom sensor measurements may represent around 5–10 cm above the sediments due to sensor protection guard, which likely over estimates DO concentrations at the SWI where steep gradients are known to occur (Schroth et al. 2015; Giles et al. 2016).

Water samples were collected at five different depths employing trace metal clean techniques (Schroth et al. 2015). In the lab, the samples were filtered following modified protocols of Shiller (2003), with size fractions operationally defined as total dissolved (< 0.45 μm) and truly dissolved (< 0.02 μm), respectively. Colloidal (0.02–0.45 μm) phases were determined by the difference in concentration between the two filtrates. Detailed sample preparation and measurement for high resolution inductively coupled plasma mass spectrometer can be found elsewhere (e.g., Schroth et al. 2015; Joung and Shiller 2016) (Supporting Information Methods). Another set of water samples were collected and filtered using a 0.45 μm pore size syringe filters (Nalgene, Thermo) for DOC, total dissolved phosphorus, soluble reactive phosphorus (SRP) determination (Silveira 2005; Schroth et al. 2015; Giles et al. 2016). Unfiltered samples were used for total P (TP) (Supporting Information Methods).

Duplicate sediment cores were collected at each site during each visit using a gravity corer, and the surface sediment ($\sim$ 1 cm) from the cores were sectioned using non-metallic core extractor. After freeze-dried and crushed finely, replicate sub-samples were collected from each sectioned sediment and were processed for extracting Fe, Mn, and P in two phases: total (aqua regia digestible) and redox sensitive (ascorbic-citrate leachable). Detailed sediment processing methods can be found in previous studies (e.g., Smith et al. 2011; Giles et al. 2016). Both the total and redox sensitive (labile) Fe, Mn and P were determined using ICP-OES (Horiba Ultima 2C) (Supporting Information). Voltammetry analyses in sediment were conducted in the field on 27th March (JD 86) and 28th (JD 87) for SP and MB, respectively. Microelectrodes were utilized to determine the redox conditions at mm resolution at the SWI in MB and SP, profiling and quantifying oxygen, Mn(II), and Fe(II) from directly above the SWI to $\sim$ 20 mm under the SWI in intact gravity cores collected at each site (Supporting Information Methods).

Results

In this result section, we mainly focused on describing 2015 data set. Detailed description of 2014 data set including winter weather, water column sensor profile and trace metals (Fe, Mn) and P in water column and sediment can be found in Schroth et al. (2015). We also note that the 2014 winter study was not designed to examine changes due to thaws, so samples were not collected immediately preceding thaw events as they were in 2015.

Winter weather

The 2015 winter was one of historical persistent cold from mid-January through mid-March with the second coldest February on record (2.2°C below the average, https://

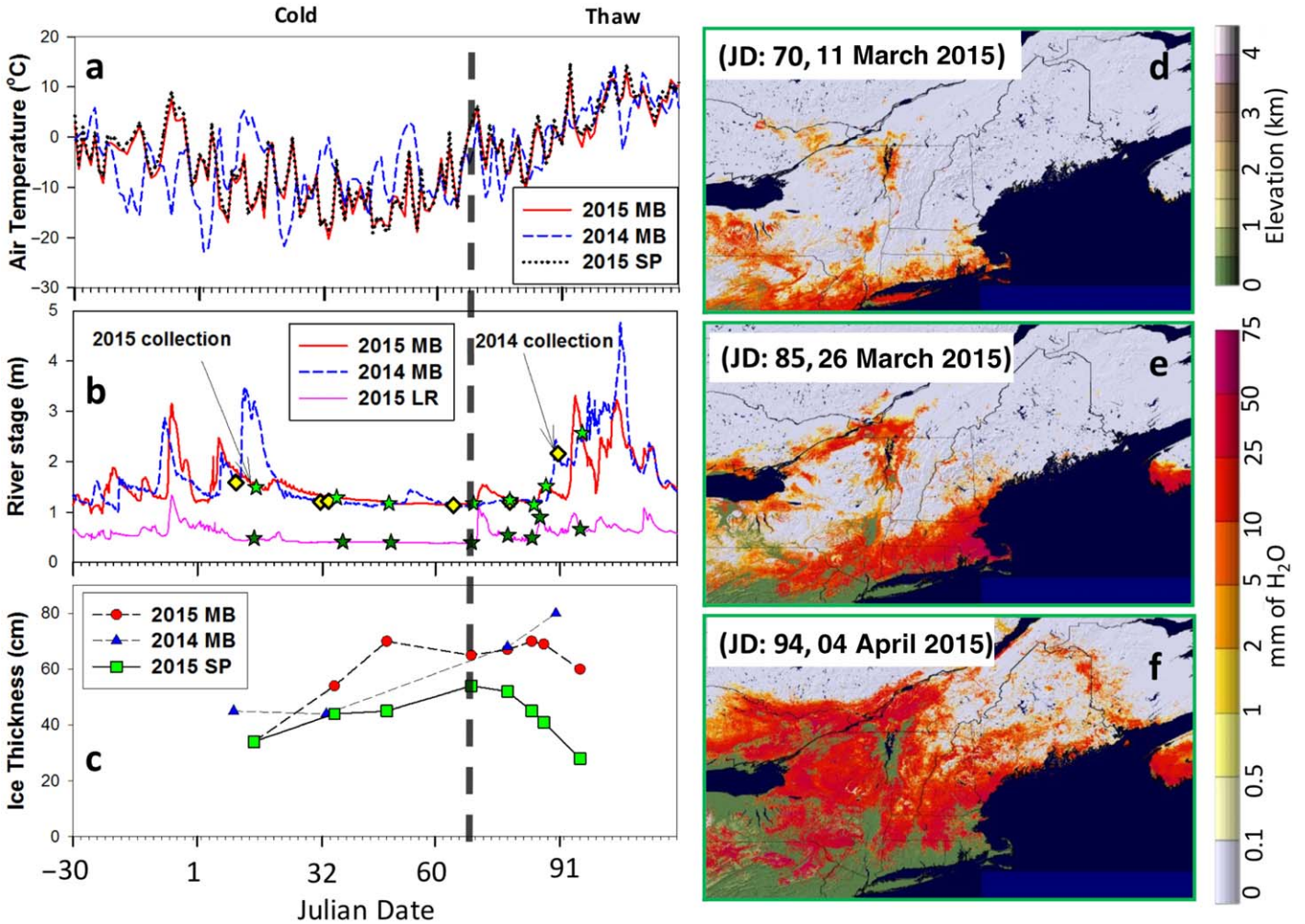

Fig. 2. Comparisons of (**a**) air temperature (daily average of the maximum and minimum temperatures), (**b**) river stage, and (**c**) ice thickness during the 2014 and 2015 winters in Missisquoi Bay (MB), and Shelburne Pond (SP). East Berkshire river stage data represent MB watershed inputs. Because of no gaged river inflow to SP, the Laplatte River (LR, 4 km away from the SP) stage data are plotted to display the watershed inputs variations in SP. All the river stage data are available at http://waterdata.usgs.gov/vt. Regional (Northeast of U.S.A.). Maps of regional snow melt distribution (right panel) on March (**d**) 11th (JD 70) and (**e**) 26th (JD 85), and (**f**) 04th April (JD 94) 2015. Figures are generated by NOAA and available at http://www.nohrsc.noaa.gov. Dates are expressed in Julian date referenced to 1/1/2015. The vertical dashed line in each graph is the time point for separating between the Cold and Thaw Periods based on snow melt occurring on JD 70.

www.ncdc.noaa.gov), which differed from the 2014 winter which had a number of intermittent above freezing air temperature periods in mid-winter (Fig. 2). Air temperature in the Champlain Valley ranged from −15°C to +10°C throughout winter 2015, with continuous below-freezing temperatures from mid-January through mid-March (Fig. 2a; termed the "Cold Period"). During the Cold Period, inputs to both MB and SP were low as indicated by river stage data; the Missisquoi and the Laplatte Rivers were frozen throughout this period (Fig. 2b). Ice thickness was 34 cm at both lake sites on the first sampling date (JD 15) and grew continuously until mid-February up to 70 cm and 45 cm in MB and SP respectively, and then remained similar in MB and reached the maximum thickness of 54 cm in SP during late March (Fig. 2c). After the first sampling date, ice thickness in SP was always less than that of MB.

After the historically persistent cold period of the 2015 winter, a series of thaw events occurred; two relatively minor and low elevation-focused thaws occurred in March (JD 70 and 85) divided by a subfreezing period, followed by the large and long duration event associated with the onset of the spring runoff period and the melting of the Green Mountain snowpack (JD 94) (Fig. 2). With warming air temperature, snow melt in the Champlain Basin occurred intermittently in mid-March (JD: 70, Fig. 2a; termed the "Thaw Period"). Remote sensing images (http://www.nohrsc.noaa.gov/nsa/index.html) indicated that during our sampling period, snow melt occurred as early as in mid-March (JD 70)

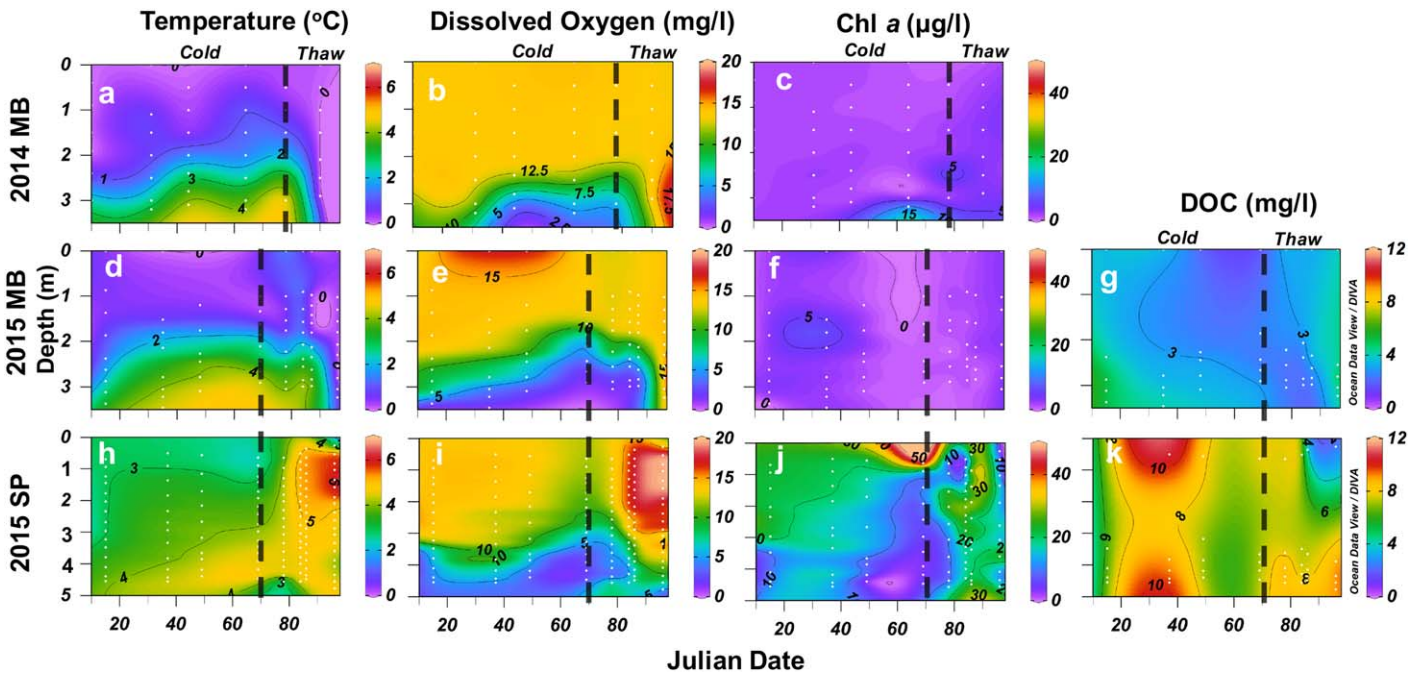

Fig. 3. Distributions of temperature, DO, Chl *a*, and DOC in 2014 (top panel) and 2015 (middle panel) winters in Missisquoi Bay (MB) and Shelburne Pond (SP, bottom panel). White dots represent sampling points. The vertical dashed line in each graph is the time point for separating between the Cold and Thaw periods based on snow melt occurring on JD 70, but the first sample collection during the Thaw Period was conducted in JD 78. For 2014 graphs, data were first published Schroth et al. (2015). No DOC measurements were made during 2014 winter sampling.

followed by a thaw in late March (JD 85) that constituted the complete depletion of the lowland snowpack of the of Champlain Valley, but had minimal impact on the relatively deep snowpack of the Green Mountains (Fig. 2d–f). These localized thaws were followed by the large regional thaw that began in early April (JD 94) with the onset of the melt of the Green Mountain snowpack. During minor thaw events, frozen rivers became active with intermittent minor increases in Missisquoi River discharge corresponding to March snow melt events, but ice break-up at the gage site did not occur until early April (Fig. 2f). During the 2014 winter in MB, there were multiple warm periods during the middle of winter, which reflected also in increased river stage. In SP, temporal trends in watershed water input (inferred from LaPlatte River) were similar to those of MB, but did not have the large peak at the early April thaw event because its watershed does not extend into the Green Mountains (like SP's basin). As air temperature increased, ice thickness at both sites began progressively thinning for the remaining period while safe sampling conditions persisted (through early April, Fig. 2c).

Water column in situ sensor data

Missisquoi Bay

The MB water column was thermally stratified during the Cold Period, with temperatures close to 0°C near the ice and 3–4°C at the bottom (Fig. 3d and Supporting Information Table 2). DO was also strongly stratified in MB during the Cold Period (Fig. 3e). The bottom water DO was consistently suboxic and this zone expanded further into the water column over the Cold Period. Chl *a* concentrations were low and hovered around the detection limit of the sensor throughout the winter (Fig. 3f). DOC was generally < 156 μmol kg^{-1} and decreased through the Cold Period (Fig. 3g). During the first two minor thaw events in March, temperature, DO, Chl *a*, and DOC did not change appreciably. However, after the major thaw event starting in early April (Fig. 2f), water temperature dropped and stratification was no longer evident, while DO became well-mixed throughout the water column and DOC increased (Fig. 3d–g). In comparison, while thermal and Chl *a* distributions were similar in both winters, DO was greatly depleted in winter in 2015 relative to 2014 (Fig. 2).

Shelburne Pond

During the Cold Period, thermal stratification was weaker and water temperature was 1–2°C warmer in SP than MB (Fig. 3h, and Supporting Information Table 2). DO concentrations were higher, but stratification in SP was similar to MB during the Cold Period (Fig. 3i). The relatively low DO layer also migrated progressively upward in the water column until mid-March. Unique to SP, DO concentrations in surface layer ($\sim$ 2 m) underneath the ice decreased as well, with similar temporal trends relative to bottom water DO depletion (Fig. 3i). Chl *a* concentrations in SP were in the range of 5–45 μg L^{-1} throughout the winter monitoring,

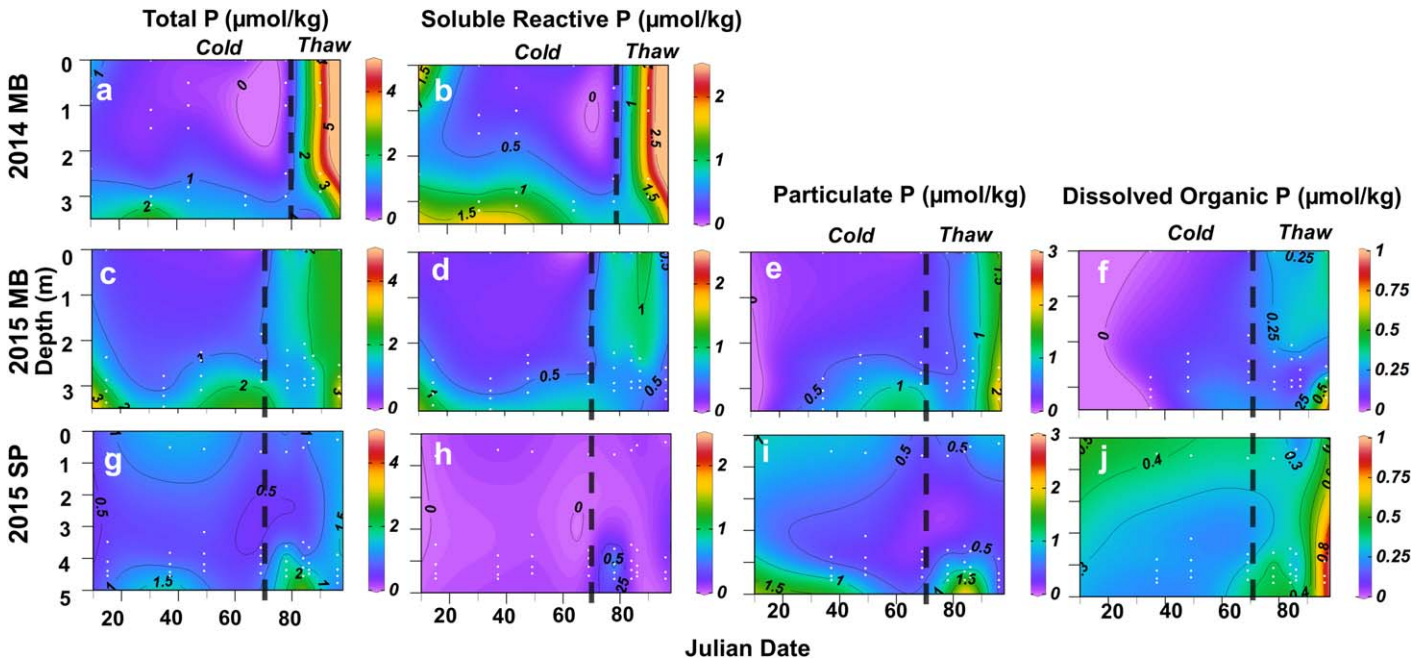

Fig. 4. Water column total (TP), soluble reactive (SRP), particulate (PP), DOP in Missisquoi Bay during 2014 (top panel) and 2015 (middle panel) winters, and Shelburne Pond (bottom panel). Note that there were no PP and DOP analysis in 2014 winter. White dots represent sampling points. Vertical dashed line in each graph is the time point for separating between the Cold and Thaw Periods based on snow melt on JD 70, but the first sample collection during the Thaw Period was conducted in JD 78. For 2014 graphs, data were first published in Schroth et al. (2015).

about 5–50 times greater than MB (Fig. 3j). DOC concentrations in SP were also higher than in MB (Fig. 3k). Unlike in MB, the localized thaw events in March coincided with the start of large changes in water column variables. Water temperature increased to 6°C and DO progressively increased to > 650 μmol kg^{-1}, with some stratification in the latter (Fig. 3h,i). Chl *a* concentration throughout the water column increased relative to preceding period and remained much higher than MB (Fig. 3j). Water column DOC in SP concentrations increased in bottom water during thaw events, while the surface concentrations decreased to the lowest concentrations observed throughout the winter monitoring (Fig. 3k).

Water column geochemistry

Missisquoi Bay

During the Cold Period, water column TP concentrations in MB ranged from 0.28 μmol kg^{-1} to 2.75 μmol kg^{-1} (Fig. 4c and Supporting Information Table 2). particulate phosphorus (PP) was the main species accounting for $> 50\%$ of TP, followed by the SRP $\sim$ 35%, and then dissolved organic phosphorus (DOP) $< 15\%$. TP, PP, and SRP concentrations were highest in bottom water during the Cold Period, with strong near surface enrichment during all thaw events (Fig. 4c–f). Truly dissolved (< 0.02 μm) Mn increased from 0.5 μmol kg^{-1} to 38 μmol kg^{-1} in bottom waters during the Cold Period (Fig. 5d). Colloidal (0.02–0.45 μm) and truly dissolved Fe in 2015 also varied across wide ranges, 0.2–4 μmol kg^{-1} and < 0.05–0.15 μmol kg^{-1}, respectively, with bottom water enrichment (Fig. 5e,f). During this period, the proportion of truly dissolved Fe relative to total dissolved Fe (< 0.45 μm) decreased from 52% to $< 3\%$. Distribution and concentration of P in 2015 were similar to those of 2014, but Mn was enriched. However, early Fe distribution were very different with being depleted in the 2015 winter relative to the 2014 winter, and later, Fe distributions were similar between winters.

During the thaw events, all P species concentrations (depth integrated) in MB increased relative to previous periods, particularly in the surface layer during the minor thaws of March. Bottom water TP concentrations did not change during early thaw events, but increased significantly on the last sampling event with the highest concentrations at 3.5 μmol kg^{-1} (Fig. 4c and Supporting Information Table 2). Unlike the Cold Period, SRP was responsible for $> 50\%$ of TP during the Thaw Period. There was also a clear increase in PP throughout the water column during thaw events with the highest proportion and concentration during the last thaw (Fig. 4e). Dissolved organic P was at its lowest proportions during thaw events, though concentrations increased at these thaw events relative to the Cold Period (Fig. 4f). Bottom water truly dissolved Mn decreased during the Thaw Period (Fig. 5d). Note that we did not measure truly dissolved fractions on our last sampling date, but truly dissolved Mn and the colloidal Fe are typically the dominant < 0.45 size fractions respectively in this as well as

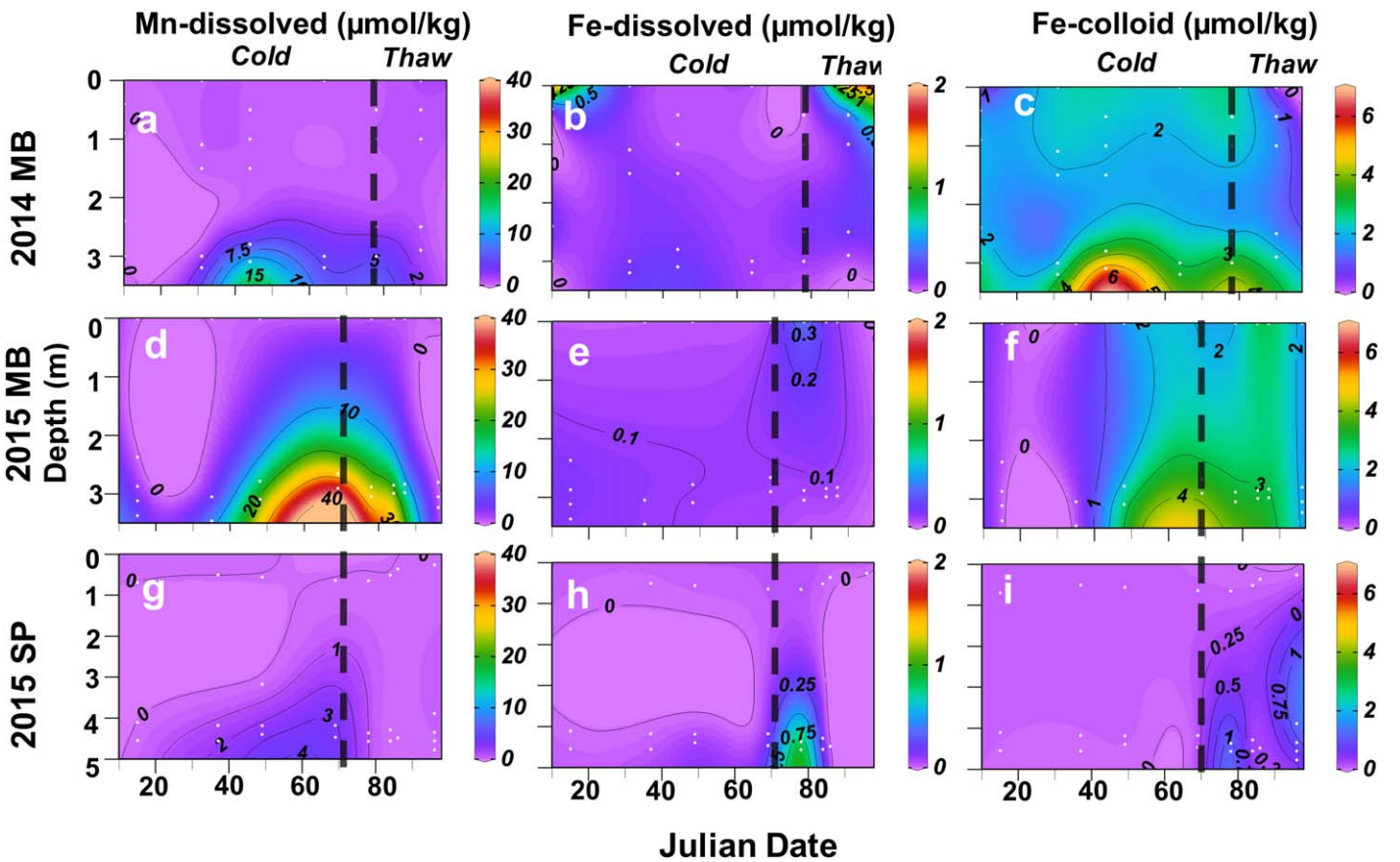

Fig. 5. Water column "truly" dissolved Mn, colloidal and "truly" dissolved Fe under ice in 2014 (top panel) and 2015 (middle panel) winters in Missisquoi Bay (MB) and in Shelburne Pond (SP) (bottom panel). Note that we have not determined truly dissolved (< 0.02 μm) Fe and Mn phases in 6th April (JD 96) samples, and thus, colloidal (0.02–0.45 μm) Fe and Mn in 6th April (JD 96) shown here are the total dissolved (< 0.45 μm) phase. The vertical dashed line in each graph is the time point for separating between the Cold and Thaw Periods based on snow melt on JD 70, but the first sample collection during the Thaw Period was conducted in JD 78. For 2014 graphs, data were first published in Schroth et al. (2015). White dots represent sampling points.

other freshwater systems (Stolpe et al. 2010; Schroth et al. 2015). During localized thaw events, colloidal Fe increased relative to the Cold Period but decreased during the regional thaw (Fig. 5f). Surface water enrichment in truly dissolved Fe was observable in thaw events when appropriate filters were available, while systematic variation of truly dissolved Fe at the bottom was not evident during thaws. In comparison, distributions of Fe, Mn, and P after the thaw events in winter were very similar.

Shelburne Pond

Water column TP concentrations in SP ranged from 0.49 μmol kg^{-1} to 1.15 μmol kg^{-1} during the Cold Period, slightly lower than in MB (Fig. 4g and Supporting Information Table 2). During this time, PP and DOP in SP were the dominant pools of P, accounting for $\sim$ 55% and 35% of TP, respectively (Fig. 4). Proportions of SRP was < 10% of TP with concentrations frequently < 0.15 μmol kg^{-1}, close to our detection limit (0.05 μmol kg^{-1}). Bottom water P concentrations (in all forms) in SP were generally higher than surface concentrations. Water column truly dissolved Mn in SP ranged from 0.1 μmol kg^{-1} to 3.8 μmol kg^{-1} during the Cold Period (Fig. 5g); an order of magnitude lower than those of MB during the same period. Weak vertical stratification and bottom water enrichment over time was evident in truly dissolved Mn (Fig. 5g). Colloidal Fe in SP was enriched in bottom water, but an order of magnitude lower than MB (Fig. 5i), while truly dissolved Fe concentrations in SP were comparable to MB except on JD 79, which the bottom water concentration was much higher than MB (Fig. 5h).

During the Thaw Periods, the TP concentrations in SP increased relative to the end of the Cold Period (Fig. 4g and Supporting Information Table 2). Among the P pools, PP and DOP drove the increase in TP during the thaw events with DOP proportions close to 60% of TP (Fig. 4g–j). During the thaw events, truly dissolved Mn concentrations decreased relative to the Cold Period (Fig. 5g). Conversely, bottom water colloidal Fe increased during this time, but concentrations remained much lower than those observed in MB (Fig. 5i). Bottom water truly dissolved Fe increased during the first thaw event, but then decreased during subsequent thaws (Fig. 5h).

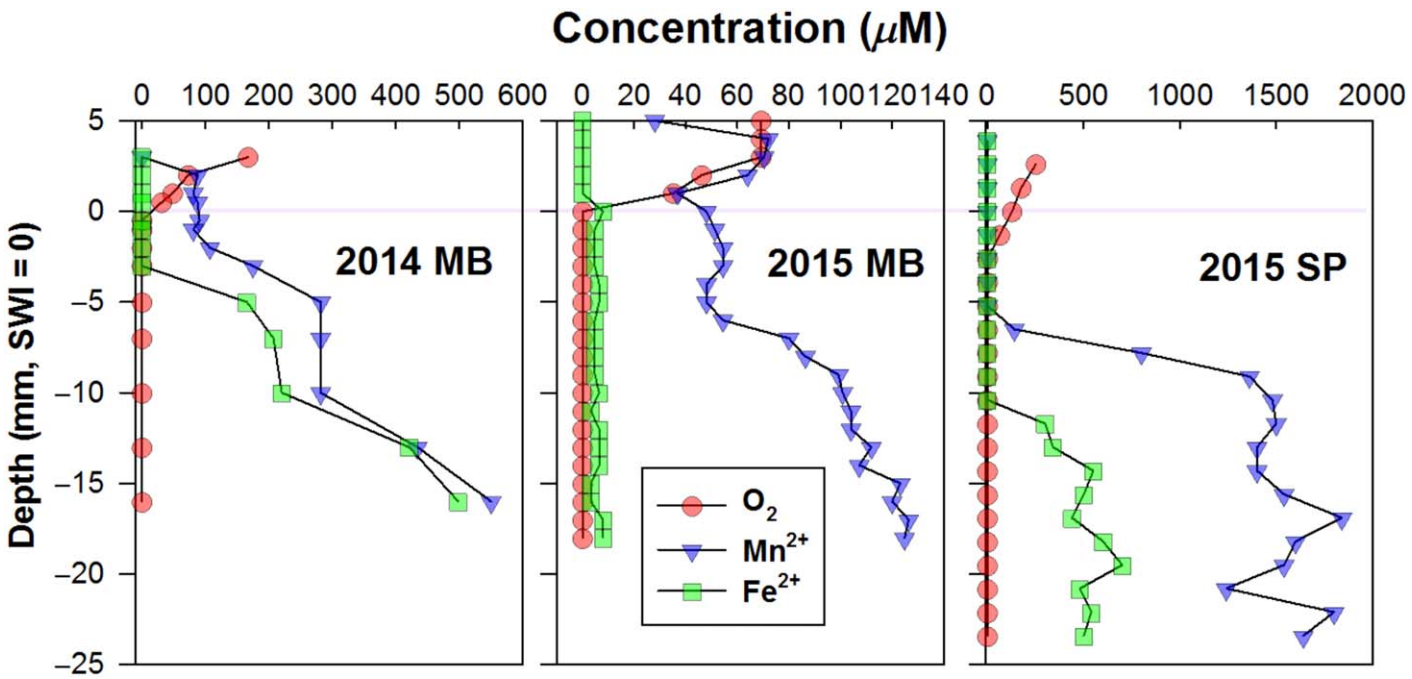

Fig. 6. Microscale vertical profiles of O_2, Fe^{2+}, Mn^{2+} determined by voltammetry in waters above the SWI and pore waters below the SWI in Missisquoi Bay (MB), and Shelburne Pond (SP). Voltammetry analysis was made 27th March (JD 86) and 28th (JD 87) 2015. Zero (0) depth indicates sediment-water interface (SWI). For 2014 graphs, data were first published in Schroth et al. (2015). Standard deviations for the measurements were less than 5%.

SWI voltammetry profiles

In MB, DO concentrations were comparable to corresponding bottom water sonde estimates, and were below detection limit at and below the SWI (Fig. 6). Mn(II) concentrations were elevated in bottom water and comparable to concurrent ICP-MS measurements of truly dissolved Mn (25 μM vs. 12 μM, respectively). Iron (II) was below detection limits in bottom water above the SWI and consistently low throughout the pore-water profile with concentrations (5–10 μM). In contrast, the pore-water concentrations of Fe and Mn in 2015 were at least 2–10 times lower than the concentrations in 2014. In SP, measurable DO penetrated well below the SWI (Fig. 6). Neither Fe(II) or Mn(II) were detectable in bottom water in SP, which also agrees with the ICP-MS concentrations. In SP pore-water profiles, both Mn(II) and Fe(II) increase with depth, albeit well below the SWI, with Mn becoming detectable at a shallower depth than Fe (Fig. 6).

Sediment geochemistry

Missisquoi Bay

Our analysis of sediment time series will focus on data from JD 15 through JD 87 while DO and thermal stratification were retained and changes in concentration are assumed to be primarily due to internal cycling, rather than the large riverine input of particulates detected during the large melt event during JD 96 where interpretation is more challenging due to the addition of external loading of riverine sediment. Surface sediment (0–1 cm) redox sensitive (ascorbic-citrate extractable) Fe concentrations in MB declined overall between (JD 15–87), whereas total aqua regia Fe remained relatively constant over the same time (Table 2 and Supporting Information Fig. 1). Sedimentary redox sensitive and total aqua regia Mn concentrations in MB sediment were highest on JD 15 but then decreased on JD 35 and subsequently remained relatively constant. Sediment redox sensitive P exhibited a net decrease across the winter, but fluctuations in concentrations between the JD 15 and JD 87 were often within the standard error of our measurements, with a similar trend in aqua regia P inventories. Molar ratios of aqua regia Fe : P ranged from 28 to 36, but did not exhibit systematic temporal variability. The percent organic carbon in these sediments hovered between 4% and 5% throughout the winter. Sediment redox sensitive Fe, Mn, and P distributions in 2015 winter were somewhat different from 2014 distributions, which increased over the course of the winter (Table 2 and Supporting Information Fig. 1).

Shelburne Pond

The concentrations of sediment redox sensitive Fe, Mn, and P under ice in SP were much lower than those of MB sediments (Table 2 and Supporting Information Fig. 1). Concentrations of redox sensitive Fe and Mn in surface sediment in SP remained relatively stable during the Cold Period,

Table 2. Concentrations of ascorbate-citrate-extractable redox sensitive and aqua regia total digestible P, Fe, and Mn of the 0–1 cm depth sediments from Missisquoi Bay in 2014 and 2015, and Shelburne Pond in 2015. JD represents Julian Date. OC stands for organic contents (%). Standard error is also presented. Unit is mg kg^{-1}.

Ascorbate-citrate-extractable (Redox-sensitive)

Missisquoi Bay												Shelburne Pond					
Date						Date						Date					
2014	JD	P	Fe	Mn	Fe* (%)	2015	JD	P	Fe	Mn	Fe* (%)	2015	JD	P	Fe	Mn	Fe* (%)
1/10	10	0.6 ± 0.2	3.1 ± 1.3	0.3 ± 0.2	10.3	1/15	15	0.622 ± 0.013	8.4 ± 0.4	1.12 ± 0.02	19.2	15/1	15	0.330 ± 0.004	1.19 ± 0.02	0.190 ± 0.003	5.1
1/31	31	0.7 ± 0.1	9.3 ± 1.7	0.8 ± 0.3	35.3	2/4	35	0.489 ± 0.009	8.9 ± 0.2	0.40 ± 0.01	17.5	6/2	37	0.244 ± 0.005	0.98 ± 0.02	0.244 ± 0.002	4.6
2/2	33	0.9 ± 0.1	10.5 ± 2.3	1.0 ± 0.5	34.7	2/17	48	0.525 ± 0.005	6.5 ± 0.1	0.40 ± 0.01	14.7	18/2	49	0.343 ± 0.004	1.11 ± 0.01	0.249 ± 0.002	4.7
3/5	64	1.0 ± 0.2	12.4 ± 2.9	1.1 ± 0.6	34.7	3/10	69	0.615 ± 0.011	6.9 ± 0.2	0.51 ± 0.01	15.4	10/3	69	0.314 ± 0.007	1.06 ± 0.02	0.243 ± 0.002	4.9
3/19	78	1.0 ± 0.3	13.6 ± 4.4	1.2 ± 0.7	35.7	3/19	78	0.357 ± 0.006	4.5 ± 0.1	0.57 ± 0.04	11.6	19/3	78	0.257 ± 0.004	1.13 ± 0.01	0.409 ± 0.014	5.3
3/31	90	1.1 ± 0.1	14.1 ± 2.6	1.3 ± 0.7	31.3	3/25	84	0.443 ± 0.006	5 ± 0.1	0.45 ± 0.01	13.2	25/3	84	0.396 ± 0.007	1.4 ± 0.02	0.347 ± 0.004	6.5
—	—	—	—	—	—	3/28	87	0.461 ± 0.008	5.6 ± 0.5	0.4 ± 0.01	13.9	27/3	86	0.276 ± 0.007	0.99 ± 0.03	0.325 ± 0.004	4.7
—	—	—	—	—	—	4/6	96	0.398 ± 0.009	5.1 ± 0.1	0.62 ± 0.01	13.7	6/4	96	0.215 ± 0.004	0.68 ± 0.01	0.292 ± 0.004	3.6

Aqua regia total digestible

Missiquoi Bay													Shelburne Pond						
Date						Date							Date						
2014	JD	P	Fe	Mn	Fe:P	2015	JD	P	Fe	Mn	OC (%)	Fe:P	2015	JD	P	Fe	Mn	OC (%)	Fe:P
1/10	10	1.2 ± 0.1	30.1 ± 2.1	1.3 ± 0.3	25.1	1/15	15	1.55 ± 0.08	43.5 ± 1.7	2.1 ± 0.2	5.3	28.1	15/1	15	1.4 ± 0.12	22.28 ± 1.21	0.43 ± 0.04	19.8	15.9
1/31	31	1.1 ± 0.0	26.3 ± 1.4	0.9 ± 0.0	24.9	2/4	35	1.41 ± 0.41	50.6 ± 14.3	0.8 ± 0.2	3.7	35.9	6/2	37	1.62 ± 0.15	21.42 ± 1.22	1.02 ± 0.71	22.9	13.2
2/2	33	1.2 ± 0.2	30.2 ± 5.9	1.1 ± 0.2	25.8	2/17	48	1.49 ± 0.21	43.8 ± 6.5	0.9 ± 0.2	3.8	29.5	18/2	49	1.63 ± 0.15	23.72 ± 1.47	0.70 ± 0.52	20.1	14.5
3/5	64	1.4 ± 0.2	35.6 ± 6.9	1.3 ± 0.4	26.4	3/10	69	1.56 ± 0.06	44.7 ± 1.7	1.3 ± 0.1	4.8	28.7	10/3	69	1.36 ± 0.01	21.7 ± 1.21	0.67 ± 0.30	24	16
3/19	78	1.3 ± 0.2	38.1 ± 1.3	1.2 ± 0.4	29.9	3/19	78	1.29 ± 0.09	39.1 ± 3.4	1.1 ± 0.4	5.5	30.4	19/3	78	1.58 ± 0.01	21.2 ± 0.35	0.99 ± 0.38	22.2	13.4
3/31	90	1.5 ± 0.3	45.1 ± 2.0	1.3 ± 0.4	29.7	3/25	84	1.30 ± 0.06	38.1 ± 2.3	1.0 ± 0.3	5.4	29.3	25/3	84	1.78 ± 0.17	21.68 ± 0.64	0.88 ± 0.16	23.6	12.2
—	—	—	—	—	—	3/28	87	1.12 ± 0.24	40.4 ± 6.9	0.7 ± 0.2	4.8	36.2	27/3	86	1.35 ± 0.24	20.92 ± 4.18	1.15 ± 0.69	17.6	15.5
—	—	—	—	—	—	4/6	96	1.01 ± 0.10	37.2 ± 1.9	1.1 ± 0.5	5.1	36.9	6/4	96	1.16 ± 0.02	19.16 ± 0.88	1.13 ± 0.36	20.3	16.5

* Fe (%) is the percentage of labile Fe over total (Aqua regia) Fe in sediment.

whereas redox sensitive P concentrations were variable throughout the sampling period with a net decrease between the beginning and end of the winter. Aqua regia derived concentrations of P in SP's surface sediment were similar to those of MB, whereas Mn concentrations were slightly less and Fe concentrations of SP were roughly half those of MB. Percent organic matter in SP were 4–5 times those of MB, hovering between 20% and 24%, while total Fe : P molar ratios were much lower than MB in a range of 13–16. Temporal variability in all aqua regia pools tended to be within the standard error of each extraction measurement, with the exception of Mn which exhibited enrichment over the course of the Cold Period.

Discussion

Persistent cold period

Historical persistent cold of the 2015 winter (Fig.2) resulted in a prolonged period of minimal watershed input and riverine forcing of circulation, mixing, and geochemical loading in both MB and SP systems (Fig. 2). As such, biogeochemical dynamics were primarily driven by internal lake processes over this time period in both systems. Despite the similar winter weather in the region, ice was thicker at MB over the course of the winter where extensive heat loss, due to its large surface area, promoted thickening of overlying ice and strong thermal stratification (Bruesewitz et al. 2015) (Fig. 2). Conversely, weaker thermal stratification and thinner ice cover of SP relative to MB resulted in less heat loss in the relatively small SP system and perhaps more convective mixing (Kelley 1997). Ramifications of these physical differences are significant for under ice ecology and biogeochemistry, as variable thickness of ice and thermal configuration impact other critical parameters such as light availability, oxygen profiles, SWI redox chemistry, and thaw hydrodynamics—all critical drivers of nutrient and metal behavior in the under ice environment (Bertilsson et al. 2013; Bruesewitz et al. 2015; Schroth et al. 2015).

Persistent suboxic conditions observed in bottom water of MB throughout the winter generated high and progressively increasing concentrations of truly dissolved Mn and P, and subsequent enrichment in colloidal Fe, all due to the reductive dissolution of Fe/Mn (oxy)hydroxides near the SWI (Schroth et al. 2015; Giles et al. 2016). This loading mechanism was independently confirmed by the concentration profile of DO and Mn(II) around the SWI (Figs. 5, 6), as well as initial decreases in redox sensitive Mn and P concentration in sediments (Supporting Information Fig. 1). Preceding bottom water enrichment of Mn (relative to Fe) in MB is consistent with the "redox ladder" concept, with release of Mn prior to Fe as the redox front progresses upward through the SWI as time under ice and persistent cold increases (Lovley 1991; Davison 1993). Initial sediment loading of reactive P concurrent with initial Mn phase dissolution also agrees with previous summer studies focused on the onset of internal P loading (Pearce et al. 2013; Giles et al. 2016). Expansion and persistence of low DO conditions due to lack of physical mixing and oxygen diffusion from the atmosphere allowed Mn concentrations to increase in the bottom water over time and expand vertically as winter progressed. In comparison to the 2014 winter, as well as multiple field campaigns during summer blooms (Smith et al. 2011; Isles et al. 2015; Giles et al. 2016), the continuous suboxic conditions of bottom water DO during the Cold Period were the most persistent ever measured at MB. This indicates that particularly cold winters that limit physical mixing and SWI reoxygenation can expose shallow sediments to prolonged periods of reducing conditions, the duration of which (months) is simply not feasible in other seasons due to more active mixing and surficial oxygen diffusion. Furthermore, the truly dissolved Mn and TP concentrations in bottom water during the Cold Period were higher and expanded further from the SWI due to the historical persistent cold of 2015 (Fig. 2). Thus, the extent of this zone and its relative enrichment in solutes must be sensitive to the duration of persistent subfreezing air temperatures.

The lack of colloidal Fe throughout the MB water column during the first two sampling events was surprising, as in 2014 (Schroth et al. 2015), colloidal Fe was ubiquitous at consistently high concentrations throughout the Cold Period (Fig. 5). We attribute an initial dearth of water column colloidal Fe in 2015 to bay-wide flushing from the rapid and expansive melt of a relatively deep December snowpack preceding initial sampling events (Fig. 2 and Supporting Information Fig. 2). This was captured by high southward velocities measured by our Acoustic doppler current profiler (ADCP) array, (Supporting Information Fig. 3) and can be inferred by the low conductivity of the bay identical to that of the river. Yet the reemergence of colloidal Fe throughout the under ice water column by JD 48 suggests that this pool can be relatively rapidly replenished under persistent subfreezing conditions, but lags the build-up of Mn and P in bottom water, likely due to re-precipitation of Fe(oxy)hydroxides before the Fe redox front has migrated above the SWI (Schroth et al. 2015). The time lag for Fe release was independently supported by sediment time series, where decreases in redox sensitive Fe were not detected until the third sampling event. Iron data from MB in 2014 and 2015 suggest that consistent subfreezing conditions promote buildup of a large pool of Fe (oxy)hydroxide colloids in the under ice water column, but dynamics are highly sensitive to winter weather and a time lag may be necessary for this pool to redevelop after a large flushing event. Increases in colloidal relative to truly dissolved Fe over time indicate rapid oxidation of sediment derived Fe(II) in bottom water, forming an expansive pool of concentrated colloidal Fe(oxy)-hydroxides in the under ice water column (Fig. 5). This could promote the observed repartitioning of bottom water

P from SRP to PP in MB, and enrichment of bottom water in P-rich Fe(oxy)hydroxide colloids and particulate phases. Similar development of P-rich Fe(III) flocs has been observed under fluctuating redox condition across riparian interfaces (Baken et al. 2015), and total Fe to P ratios across the sediment time series are in a range where Fe behavior is thought to drive P dynamics (Supporting Information Fig. 1) (Søndergaard et al. 2003).

While P and Fe behavior during the Cold Period of 2014 and 2015 in MB was clearly redox driven, the net effect of each winter on the accumulation or depletion of the redox sensitive pool in sediment differed substantially. Lower and progressively decreasing concentrations of redox sensitive Fe, Mn, and P in the 2015 Cold Period contrast higher concentrations and progressive enrichment in 2014 (Schroth et al. 2015) (Supporting Information Fig. 1). Thus, the redox sensitivity of P and Fe in surface sediments at the end of winter must be sensitive to the persistence and severity of subfreezing temperatures. Conversely, total pools of each constituent are quite comparable (Table 2), suggesting that winter weather may impact the partitioning of metals and P in the sediment more than the total pool. Flux estimates of redox sensitive Fe, Mn, and P to the overlying water column (following Smith et al. 2011) were broadly consistent with water column concentrations (Supporting Information Table 3). Observed discrepancy between sediment and water column data was anticipated due to: (1) re-precipitation of deep sediment derived solutes in surface sediment (Schroth et al. 2015), (2) partitioning into different phases (e.g., comparable total concentrations throughout), (3) colloidal flocculation/re-deposition, (4) sediment spatial heterogeneity, and (5) difficulty sampling steep concentration gradients around the SWI (e.g., Smith et al. 2011). Nonetheless, inter-annual variability of sediment pools, particularly when coupled with concurrent variability in voltammetry and water column profiles of both winters (Fig. 6), suggests that the severity/persistence of cold exerts a strong control on SWI redox dynamics. This impacts the inventory and distribution of reactive species of Fe, P, and Mn in water column and sediment profiles by controlling the position of the redox front, and therefore the flux and partitioning of Fe, Mn, and P in the water column and sediment.

The lake-watershed configuration of SP produced a very different under ice biogeochemical system relative to MB under the same Cold Period. Shelburne Pond was much more biologically active with relatively high concentrations of phytoplankton near the upper portion of the water column, less thermal and DO stratification, and a more oxidized SWI (Fig. 3). While minor bottom water enrichment of all species was detected, less reducing conditions around the SWI resulted in lower concentrations of colloidal Fe and truly dissolved Mn due to less reductive release of Fe and Mn from sediment (Figs. 4, 5), typical of an oxygenated environment (Davison 1993; Martin 2005). Consistent and low concentrations of redox sensitive Mn, Fe, and P in sediment underneath the ice further support this contention (Table 2 and Supporting Information Fig. 1), as does the highly oxygenated SWI (Fig. 6). The abrupt increase in SP sediment pore water Mn(II) and Fe(II) concentration with depth to concentrations much higher than ambient bottom water concentrations in SP or any sediment pore water measured in MB, indicates that deep oxygenated sediment acts as a highly effective barrier suppressing diffusion of sediment-derived solutes into the SP water column.

Water column iron size partitioning with comparable concentrations of colloidal and "truly dissolved" Fe in SP, differed considerably from concurrent MB waters that bore an order of magnitude more colloidal Fe across depths (Fig. 5). Considering the more reducing SWI and more expansive region of DO depleted water in MB, one might anticipate more dissolved Fe, yet the opposite was the case. This could be due to higher concentration of organic colloids sourced in the more organic rich sediments and water column of SP, coupled with less internal loading of rapidly oxidized aqueous Fe(II) from more oxidized sediments. Our operational definition of truly dissolved Fe consists primarily of organically complexed colloids in the oxidizing circumneutral conditions of the SP water column, whereas our colloidal size fraction primarily consists of mineral Fe-(oxy)hydroxides (Shiller 2003; Stolpe et al. 2010), the dominant fraction of Fe in the organic poor MB system. Thus, cross site comparison of Fe data indicates that these physical differences and their cascading impacts exert a strong control on size partitioning (and inferred speciation) and vertical distribution of Fe in the under ice water column, even under the same ambient meteorological conditions and suppressed watershed input.

Under ice phytoplankton, barely detectable in MB under any ice thickness in either year, had an important impact on SP water column P dynamics. Low SRP concentrations must have been due to rapid consumption by phytoplankton coupled with less internal release from a more oxidized SWI bearing sediment less enriched in redox sensitive P. Yet during the same period, the proportions of PP and DOP were greater in SP relative to those of MB, suggesting that biological consumption and remineralization was driving P cycling in the SP under ice water column (rather than Fe redox driven chemical cycling in MB). Indeed, the SP sediment Fe : P ratio hovered around or slightly below 15, a critical threshold under which Fe cycling is thought to be decoupled from P mobility in sediment-water systems (Supporting Information Fig. 1) (Søndergaard et al. 2003). High organic content of SP sediments (25%) relative to MB sediments ($\sim$ 5%) (Table 2) also suggests that the productive SP under ice ecosystem, coupled with minimal mineral resupply due to lack of riverine input, results in a system where organic matter mineralization appears to play a dominant role in internal cycling of metals and P relative to SWI redox conditions (Lovley 1991; Manasypov et al. 2015). This is supported by

the increased proportion of Fe and P in SP associated with species that would be sourced in the mineralization of organic matter; truly dissolved Fe complexed to organic ligands and DOP respectively. In general, sediment and solute under ice time series demonstrate that Fe and P behavior is decoupled in SP, but fully coupled in MB during the Cold Period. Such variability in under ice drivers of metal and P cycling should be expected globally (e.g., Søndergaard et al. 2003), even when considering systems of similar trophic state exposed to the same winter weather. Furthermore, SP sediment compositional data (Table 2) suggests that the Cold Period had very little impact on the concentration or partitioning of Fe, Mn, and P in sediment, in contrast to dynamic behavior observed in MB during both 2014 and 2015. Thus, the impact of the under ice period on sediment pools of Mn, Fe, and P leading into productive spring periods is highly variable in space, related not only to winter weather, but also driven by the cascading impacts of lake-watershed physical configuration on under ice biogeochemical and ecological dynamics.

System response to thaw events

Thaw events had distinct impacts on MB hydrodynamics and biogeochemistry that varied by thaw severity and provenance. Preservation of DO and thermal stratification, as well as bottom water enrichment of sediment-sourced redox sensitive solutes and colloids, during minor thaws suggests that thaw impact on mixing and SWI redox conditions was minimal. This was further confirmed by no appreciable differences in the flow velocity between minor thaws and preceding periods (Supporting Information Fig. 3). Thus, minor thaws do not appear to interrupt internal chemical loading associated with preceding cold periods. Strong near surface enrichment of SRP and truly dissolved Fe confirms that these solute species are characteristic of thaw events, also observed in 2014 winter thaws (Figs. 4, 5) (Schroth et al. 2015). Enrichment location indicates that the plume of cold river water input to MB during minor midwinter thaws is constrained just below the ice where near zero (°C) water in the upper water column of similar density is positioned in the bay's antecedent thermal configuration. Meltwater provenance explains the strong enrichment of the river water plume in SRP, as the Champlain Valley lowlands bear most of the P-amended agricultural portion of the watershed that is typically flushed during the onset of low elevation spring melt (Fig. 2) (Rosenberg and Schroth 2017). As such, initial minor thaws may be disproportionately important in providing a highly reactive flux of P to the lake due to thaw provenance and the configuration of land practices in the Champlain Valley.

The large regional snowmelt event provided a high influx of river water sufficient in scale to break down the long-established winter thermal and DO stratification due to bay wide enhanced circulation and mixing (Figs. 2, 3, and Supporting Information Fig. 3). Different conductivity and turbidity profiles of this event were similar to concurrent river measurements of these parameters (Supporting Information Table 2), suggesting that entire water column has been impacted and displaced by river water inputs, also evident from widespread homogenous distribution of other constituents. The low and homogenous concentration profile of SRP in the lake during the large late thaw is due to the fact that most of the snowmelt and an increasing of river discharge is sourced in forested uplands of the Green Mountains, as the lowlands were devoid of snow (Fig. 2). Thus, the dominant source of river water was coming from an environment inherently low in labile P, and lowland solute rich soil waters had been recently flushed by the preceding thaws. Strong enrichment in PP throughout the water column during the large thaw event suggests these high flows delivered most of P in particulate form, whereas localized lowland thaws tended to enrich the system most in SRP. Particulate P is likely derived from erosion and sediment transport within the watershed, and to a lesser extent, perhaps sediment resuspension in the bay, consistent with previous observations during spring runoff in the Missisquoi River Basin (Rosenberg and Schroth 2017). Overall, through interpretation of MB thaw data, it is apparent that a hydrologic threshold exists, below which thaws do not offset the basic thermal and redox stratification of the water column and SWI. Consequently, thaw severity likely plays a critical role in the cumulative loads of nutrients to the lake, with system specific thresholds likely of thaw size capable of disrupting the internal geochemical drivers that control the flux of Mn, Fe, and P from sediments. Furthermore, water column composition and distribution is also strongly impacted by thaw provenance and watershed antecedent conditions. In watersheds with land-use, ecological or elevational/climatic gradients, thaws that differentially impact particular portions of the watershed and related pools of nutrients or metals may produce vastly different metal and P loads and related impacts on under ice water column chemistry.

Due to differences in lake-watershed physical configuration, coupled with differences in antecedent biogeochemical, thermal, and ecological conditions promoted during preceding Cold Period, the same meteorological events impacted the SP system differently than MB. Rapid increase in SP water column temperature during the initial thaws (Fig. 3) weakened water column thermal stratification, albeit by a completely different physical mechanism than riverine input-derived stratification break down observed in MB. Increasing Chl *a* and DO supersaturation during thaws suggests that watershed inputs of immediately bioavailable nutrients (Meixner and Bales 2003), warmer water temperatures, and more available light triggered biological production increase. This was never observed in MB, as phytoplankton were not sufficiently abundant to respond to changes in light and nutrient availability. Persistence of vertical DO depletion through thaw events

indicates that the SP SWI was not fully re-oxygenated in response to thaws, whereas the large thaw completely broke down DO stratification and thermal structure of MB due to extremely high discharge from the Missisquoi River (Fig. 3). Minimal hydrodynamic impact of thaws on SP is due to its relatively small watershed:lake area and lack of a major tributary. In addition, increases of bottom water DO, turbidity, nitrate, DOC, P, and Fe in the first thaw suggest that the plume of watershed water was transported along the bottom of SP, in contrast to MB where the same signals of early thaw enrichment tended to move along surface (Fig. 3, Supporting Information Fig. 4). The different location of the thaw water inputs at each site is driven by the different antecedent thermal structures and associated density gradients within each under ice water column, as well as input vectors (MB-large river vs. SP diffuse groundwater and snowmelt runoff). In SP, cold diffuse snowmelt presumably sinks in the relatively warm lake water and follows bathymetrically-determined flow paths. Whereas in MB, cold river water of the minor thaw events flows along the ice-water interface until the riverine input is sufficient in scale to displace the lake water and break down stratification. These analyses demonstrate that differences in system response to the same thaw events were derived from differences in antecedent conditions and lake-watershed physical configuration.

Conclusions

A number of interesting and novel conclusions regarding the poorly understood under ice biogeochemical system can be gleaned from this work. First, the inter-annual variability of under ice P, Mn, and Fe dynamics is influenced heavily by winter weather such as the severity and duration of subfreezing air temperatures vs. the timing and magnitude of thaws. The more severe and persistent periods of subfreezing temperatures, the more expansive and concentrated the pool of P, Mn, and Fe species associated with reductive release from sediment becomes in the water column. Second, components of lake-watershed physical configuration such as its lake size, depth, and watershed : lake area lead to variability in heat loss, ice thickness, light availability, thermal stratification, and biological production. This ultimately impacts the degree to which Fe and P behavior is coupled, as well as their speciation and concentration in the sediment and water column. Third, in watersheds spanning land-use/land-cover gradients, thaw provenance and timing is important for understanding impacts on receiving water chemistry. Different thaw events may activate different "hot spots" for P and metals within a watershed with consequent impact on the partitioning and concentration of metals and P delivered to the lake. Furthermore, the severity of a thaw, as well as the antecedent physical conditions within the lake, dictate thaw impact on lake hydrodynamics and its ability to disrupt SWI redox chemistry produced by periods of limited mixing under persistent cold. Projecting how a lake's biogeochemistry and ecology may respond to less frequent or persistent periods of ice cover or subfreezing temperatures coupled with changing thaw dynamics under a warmer climate requires consideration of a comprehensive array of variables related to a lake's internal and external configuration, as well as the nature of changing winter weather over time.

References

Adrian, R., N. Walz, T. Hintze, S. Hoeg, and R. Rusche. 1999. Effects of ice duration on plankton succession during spring in a shallow polymictic lake. Freshw. Biol. **41**: 621–634. doi:10.1046/j.1365-2427.1999.00411.x

Adrian, R., and others. 2009. Lakes as sentinels of climate change. Limnol. Oceanogr. **54**: 2283. doi:10.4319/lo.2009.54.6_part_2.2283

Babin, J., and E. Prepas. 1985. Modelling winter oxygen depletion rates in ice-covered temperate zone lakes in Canada. Can. J. Fish. Aquat. Sci. **42**: 239–249. doi:10.1139/f85-031

Baken, S., M. Verbeeck, D. Verheyen, J. Diels, and E. Smolders. 2015. Phosphorus losses from agricultural land to natural waters are reduced by immobilization in iron-rich sediments of drainage ditches. Water Res. **71**: 160–170. doi:10.1016/j.watres.2015.01.008

Balistrieri, L. S., J. W. Murray, and B. Paul. 1992. The biogeochemical cycling of trace metals in the water column of Lake Sammamish, Washington: Response to seasonally anoxic conditions. Limnol. Oceanogr. **37**: 529–548. doi:10.4319/lo.1992.37.3.0529

Bengtsson, L. 1996. Mixing in ice-covered lakes. Hydrobiologia **322**: 91–97. doi:10.1007/BF00031811

Bertilsson, S., and others. 2013. The under-ice microbiome of seasonally frozen lakes. Limnol. Oceanogr. **58**: 1998–2012. doi:10.4319/lo.2013.58.6.1998

Brooks, P. D., and M. W. Williams. 1999. Snowpack controls on nitrogen cycling and export in seasonally snow-covered catchments. Hydrol. Process. **13**: 2177–2190. doi:10.1002/(SICI)1099-1085(199910)13:14/15<2177::AID-HYP850>3.0.CO;2-V

Brown, J. S., E. D. Stein, D. Ackerman, J. H. Dorsey, J. Lyon, and P. M. Carter. 2013. Metals and bacteria partitioning to various size particles in Ballona Creek storm water runoff. Environ. Toxicol. Chem. **32**: 320–328. doi:10.1002/etc.2065

Bruesewitz, D. A., C. C. Carey, D. C. Richardson, and K. C. Weathers. 2015. Under-ice thermal stratification dynamics of a large, deep lake revealed by high-frequency data. Limnol. Oceanogr. **60**: 347–359. doi:10.1002/lno.10014

Catalan, J. 1992. Evolution of dissolved and particulate matter during the ice-covered period in a deep, high-mountain lake. Can. J. Fish. Aquat. Sci. **49**: 945–955. doi:10.1139/f92-105

Davison, W. 1993. Iron and manganese in lakes. Earth Sci. Rev. **34**: 119–163. doi:10.1016/0012-8252(93)90029-7

Davison, W., and G. Seed. 1983. The kinetics of the oxidation of ferrous iron in synthetic and natural waters. Geochim. Cosmochim. Acta **47**: 67–79. doi:10.1016/0016-7037(83)90091-1

Dibike, Y., T. Prowse, B. Bonsal, L. D. Rham, and T. Saloranta. 2012. Simulation of North American lake-ice cover characteristics under contemporary and future climate conditions. Int. J. Climatol. **32**: 695–709. doi:10.1002/joc.2300

Fang, X., and H. G. Stefan. 1996. Dynamics of heat exchange between sediment and water in a lake. Water Resour. Res. **32**: 1719–1727. doi:10.1029/96WR00274

Ferber, L. R., S. N. Levine, A. Lini, and G. P. Livingston. 2004. Do cyanobacteria dominate in eutrophic lakes because they fix atmospheric nitrogen? Freshw. Biol. **49**: 690–708. doi:10.1111/j.1365-2427.2004.01218.x

Gammons, C. H., W. Henne, S. R. Poulson, S. R. Parker, T. B. Johnston, J. E. Dore, and E. S. Boyd. 2014. Stable isotopes track biogeochemical processes under seasonal ice cover in a shallow, productive lake. Biogeochemistry **120**: 359–379. doi:10.1007/s10533-014-0005-z

Gilbert, B., H. Zhang, F. Huang, M. P. Finnegan, G. A. Waychunas, and J. F. Banfield. 2003. Special phase transformation and crystal growth pathways observed in nanoparticles. Geochem. Trans. **4**: 20–27. doi:10.1039/b309073f

Giles, C. D., P. D. Isles, T. Manley, Y. Xu, G. K. Druschel, and A. W. Schroth. 2016. The mobility of phosphorus, iron, and manganese through the sediment–water continuum of a shallow eutrophic freshwater lake under stratified and mixed water-column conditions. Biogeochemistry **127**: 15–34. doi:10.1007/s10533-015-0144-x

Hodgkins, G. A., I. C. James, and T. G. Huntington. 2002. Historical changes in lake ice-out dates as indicators of climate change in New England, 1850–2000. Int. J. Climatol. **22**: 1819–1827. doi:10.1002/joc.857

IPCC. 2007. Climate change 2007: Synthesis report, p. 104. *In* Core Writing Team, R. K. Pachauri, and A. Reisinger [eds.], Contribution of working groups I, II and III to the fourth assessment report of the Intergovernmental Panel on Climate Change. IPCC.

Isles, P. D., C. D. Giles, T. A. Gearhart, Y. Xu, G. K. Druschel, and A. W. Schroth. 2015. Dynamic internal drivers of a historically severe cyanobacteria bloom in Lake Champlain revealed through comprehensive monitoring. J. Great Lakes Res. **41**: 818–829. doi:10.1016/j.jglr.2015.06.006

Jackson, L. J., T. L. Lauridsen, M. Søndergaard, and E. Jeppesen. 2007. A comparison of shallow Danish and Canadian lakes and implications of climate change. Freshw. Biol. **52**: 1782–1792. doi:10.1111/j.1365-2427.2007.01809.x

Joung, D., and A. M. Shiller. 2016. Temporal and spatial variations of dissolved and colloidal trace elements in Louisiana Shelf waters. Mar. Chem. **181**: 25–43. doi:10.1016/j.marchem.2016.03.003

Karlsson, J., J. Ask, and M. Jansson. 2008. Winter respiration of allochthonous and autochthonous organic carbon in a subarctic clear-water lake. Limnol. Oceanogr. **53**: 948–954. doi:10.4319/lo.2008.53.3.0948

Kawashima, M., Y. Tainaka, T. Hori, M. Koyama, and T. Takamatsu. 1986. Phosphate adsorption onto hydrous manganese (IV) oxide in the presence of divalent cations. Water Res. **20**: 471–475. doi:10.1016/0043-1354(86)90195-8

Kelley, D. E. 1997. Convection in ice-covered lakes: Effects on algal suspension. J. Plankton Res. **19**: 1859–1880. doi:10.1093/plankt/19.12.1859

Leppäranta, M. 2014. Freezing of lakes and the evolution of their ice cover. Springer Science & Business Media.

Levine, S. N., and others. 2012. The eutrophication of Lake Champlain's northeastern arm: Insights from paleolimnological analyses. J. Great Lakes Res. **38**: 35–48. doi:10.1016/j.jglr.2011.07.007

Lini, A., S. Levine, M. L. Ostrofsky, and D. Dahlen. 2007. Trophic history of Shelburne Pond. Vermont Agency of Natural Resources.

Lovley, D. R. 1991. Dissimilatory Fe (III) and Mn (IV) reduction. Microbiol. Rev. **55**: 259–287.

Magnuson, J. J., and others. 2000. Historical trends in lake and river ice cover in the Northern Hemisphere. Science **289**: 1743–1746. doi:10.1126/science.289.5485.1743

Manasypov, R., O. Pokrovsky, S. Kirpotin, and L. Shirokova. 2014. Thermokarst lake waters across the permafrost zones of western Siberia. Cryosphere **8**: 1177–1193. doi:10.5194/tc-8-1177-2014

Manasypov, R., and others. 2015. Seasonal dynamics of organic carbon and metals in thermokarst lakes from the discontinuous permafrost zone of western Siberia. Biogeosciences **12**: 3009–3028. doi:10.5194/bg-12-3009-2015

Martin, S. T. 2005. Precipitation and dissolution of iron and manganese oxides, p. 61–81. *In* Environmental catalysis, edited by V. H.Grassian pp. 61–81, CRC Press, Boca Raton, Fla.

Meixner, T., and R. C. Bales. 2003. Hydrochemical modeling of coupled C and N cycling in high-elevation catchments: Importance of snow cover. Biogeochemistry **62**: 289–308. doi:10.1023/A:1021118922787

Nürnberg, G. K., B. D. Lazerte, P. S. Loh, and L. A. Molot. 2013. Quantification of internal phosphorus load in large, partially polymictic and mesotrophic Lake Simcoe, Ontario. J. Great Lakes Res. **39**: 271–279. doi:10.1016/j.jglr.2013.03.017

Pearce, A. R., D. M. Rizzo, M. C. Watzin, and G. K. Druschel. 2013. Unraveling associations between cyanobacteria blooms and in-lake environmental conditions in Missisquoi Bay, Lake Champlain, USA, using a modified self-organizing map. Environ. Sci. Technol. **47**: 14267–14274. doi:10.1021/es403490g

Rosenberg, B., and A. W. Schroth. 2017. Coupling of reactive riverine phosphorus and iron species during hot transport moments: impacts of land cover and seasonality. Biogeochemistry, **132**: 103–122. doi:10.1007/s10533-016-0290-9

Schroth, A. W., C. D. Giles, P. D. Isles, Y. Xu, Z. Perzan, and G. K. Druschel. 2015. Dynamic coupling of iron, manganese, and phosphorus behavior in water and sediment of shallow ice-covered eutrophic lakes. Environ. Sci. Technol. **49**: 9758–9767. doi:10.1021/acs.est.5b02057

Shiller, A. M. 2003. Syringe filtration methods for examining dissolved and colloidal trace element distributions in remote field locations. Environ. Sci. Technol. **37**: 3953–3957. doi:10.1021/es0341182

Shuter, B., C. Minns, and S. Fung. 2013. Empirical models for forecasting changes in the phenology of ice cover for Canadian lakes. Can. J. Fish. Aquat. Sci. **70**: 982–991. doi:10.1139/cjfas-2012-0437

Silveira, M. L. A. 2005. Dissolved organic carbon and bioavailability of N and P as indicators of soil quality. Sci. Agric. **62**: 502–508. doi:10.1590/S0103-90162005000500017

Smith, L., M. C. Watzin, and G. Druschel. 2011. Relating sediment phosphorus mobility to seasonal and diel redox fluctuations at the sediment–water interface in a eutrophic freshwater lake. Limnol. Oceanogr. **56**: 2251–2264. doi:10.4319/lo.2011.56.6.2251

Søndergaard, M., J. P. Jensen, and E. Jeppesen. 2003. Role of sediment and internal loading of phosphorus in shallow lakes. Hydrobiologia **506**: 135–145. doi:10.1023/B:HYDR.0000008611.12704.dd

Stolpe, B., L. Guo, A. M. Shiller, and M. Hassellöv. 2010. Size and composition of colloidal organic matter and trace elements in the Mississippi River, Pearl River and the northern Gulf of Mexico, as characterized by flow field-flow fractionation. Mar. Chem. **118**: 119–128. doi:10.1016/j.marchem.2009.11.007

Vincent, W. F. 1981. Production strategies in Antarctic inland waters: Phytoplankton eco-physiology in a permanently ice-covered lake. Ecology **62**: 1215–1224. doi:10.2307/1937286

Vincent, W. F. 2010. Microbial ecosystem responses to rapid climate change in the Arctic. ISME J. **4**: 1087. doi:10.1038/ismej.2010.108

Vermont Department of Environmental Conservation (VTDEC), and New York State Department of Environmental Conservation (NYDEC). 2014. Lake Champlain long-term water quality and biological monitoring program—Program description. Grand Isle, Vermont [accessed 2016 April 30]. Available from http://www.watershedmanagement.vt.gov/lakes/htm/lp_longterm.htm

Weyhenmeyer, G. A., T. Blenckner, and K. Pettersson. 1999. Changes of the plankton spring outburst related to the North Atlantic Oscillation. Limnol. Oceanogr. **44**: 1788–1792. doi:10.4319/lo.1999.44.7.1788

Weyhenmeyer, G. A., T. Blenckner, K. Pettersson, A. K. Westöö, and E. Willén. 2008. Increasingly ice-free winters and their effects on water quality in Sweden's largest lakes. Hydrobiologia **599**: 111–118. doi:10.1007/s10750-007-9188-9

Weyhenmeyer, G. A., T. Blenckner, K. Pettersson, D. M. Livingstone, M. Meili, O. Jensen, B. Benson, and J. J. Magnuson. 2011. Large geographical differences in the sensitivity of ice-covered lakes and rivers in the Northern Hemisphere to temperature changes. Glob. Chang. Biol. **17**: 268–275. doi:10.1111/j.1365-2486.2010.02249.x

Winston, G., B. Stephens, E. Sundquist, J. Hardy, and R. E. Davis. 1995. Seasonal variability in CO2 transport through snow in a boreal forest, p. 61–70. Proceedings of a Boulder Symposium, July 1995. IAHS Publ. no. 228.

Zaman, M. I., S. Mustafa, S. Khan, M. I. Khan, A. Niaz, and Y. Muhammad. 2013. The effects of phosphate adsorption on the surface characteristics of Mn oxides. Sep. Sci. Technol. **48**: 1709–1716. doi:10.1080/01496395.2012.756033

Acknowledgment

We thank to T. Gearhart, B. O'Malley, and A. Lini for their assistance in sample collection and perpetration. We also thank the staff at Woods Hole Oceanographic Institution (WHOI) plasma facility. This material is based upon work supported by the National Science Foundation under grants EPS-1101317, EPS-IIA1330446, OIA1556770, EAR-1561014, and a Vermont EPSCoR Pilot Grant. Any opinions, findings, and conclusions or recommendations expressed in this material are those of the author(s) and do not necessarily reflect the views of the National Science Foundation or Vermont EPSCoR.

Conflict of Interest

None declared.

Submitted 12 May 2016
Revised 13 August 2016; 19 December 2016
Accepted 09 January 2017

Associate editor: Caroline Slomp